NANO LETTERS

Letter

pubs.acs.org/NanoLett

High-Efficiency Second-Harmonic Generation from Hybrid Light-Matter States

Thibault Chervy,[†] Jialiang Xu,[*,‡,§] Yulong Duan,[§] Chunliang Wang,[†] Loïc Mager,[∥] Maurice Frerejean,[§] Joris A. W. Münninghoff,[§] Paul Tinnemans,[§] James A. Hutchison,[†] Cyriaque Genet,[†] Alan E. Rowan,[§,⊥] Theo Rasing,[§] and Thomas W. Ebbesen[*,†]

[†]ISIS and icFRC, University of Strasbourg and CNRS, 8 allée Gaspard Monge, 67000 Strasbourg, France

[‡]School of Chemical Engineering and Technology, Tianjin University, Yaguan Road 135, 300350 Tianjin, People's Republic of China

[§]Institute for Molecules and Materials (IMM), Radboud University, Heyendaalseweg 135, 6525AJ Nijmegen, The Netherlands

[∥]IPCMS, University of Strasbourg and CNRS, 23 rue du Loess, 67034 Strasbourg, France

[⊥]Australian Institute for Bioengineering and Nanotechnology (AIBN), The University of Queensland, Brisbane, Queensland 4072, Australia

Supporting Information

ABSTRACT: We report a novel approach to modify the second order nonlinear optical (NLO) susceptibility of organic nanofiber crystals by hybridization with the optical modes of microcavities in the strong coupling regime. The wavelength dependence of the SHG efficiency displays two intense peaks corresponding to the so-formed light-matter hybrid states. Our results demonstrate an enhancement of the resonant SHG efficiency of the lower polariton by 2 orders of magnitude for the collectively coupled molecules as compared to that of the same material outside the microcavity. This study is a proof of principle that opens a new direction for NLO of organic materials in subwavelength resonators.

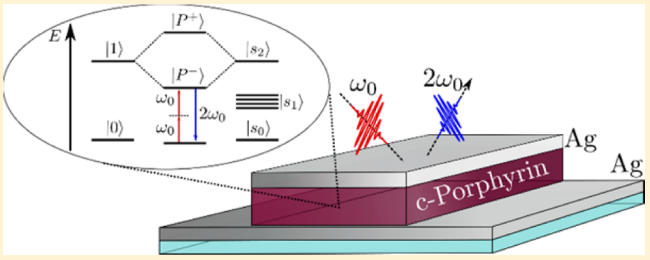

KEYWORDS: *Second harmonic generation, strong coupling, cavity, polariton state, self-assembly*

Second-harmonic generation (SHG) remains one of the most widely applied nonlinear optical (NLO) effects since its first observation over a half-century ago.[1−5] Organic SHG active materials have attracted considerable attention due to the diverse choice of molecular materials and their efficient second-order NLO response.[6] Furthermore, the supramolecular self-assembly of these molecular systems offers opportunities for the construction of NLO materials with well-defined architectures at the subwavelength scale, with potential applications in integrated photonic circuits.[7−9] However, photodegradation and harmonic reabsorption have so far limited their use in devices. Moreover, the effective translation of the molecular hyperpolarizabilities of the NLO dyes to the corresponding material susceptibilities remains a great challenge.

Light-matter interaction in a confined electromagnetic environment can reach a regime where the energy is coherently exchanged between light and matter in a reversible way.[10] In this strong light-matter coupling regime, a given electromagnetic mode hybridizes with a material resonance, giving rise to exciton−polariton eigenstates (noted |P+> and |P−>) separated in energy by the so-called Rabi splitting as illustrated in Figure 1. This regime can only be reached if the light-matter energy exchange rate, corresponding to the coupling frequency, exceeds all possible relaxation rates of the entities to be coupled. Although this is a very strong constraint for a single absorber coupled to a resonant optical cavity mode, it has been demonstrated[11] that coupling an ensemble of N absorbers to the same optical mode increases the coupling frequency by a factor $\sqrt{N}$, allowing the strong coupling regime to be reached

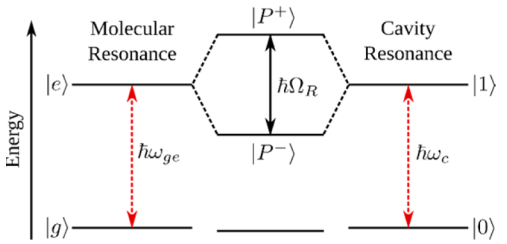

Figure 1. Schematic representation of the strong coupling regime between a molecular resonance (|g> to |e> transition, frequency ω_{ge}) and a cavity resonance at frequency ω_c (transition from vacuum state (|0> to one-photon state |1>). The light-matter strong coupling gives rise to exciton-polariton eigenstates |P+> and |P−> separated in energy by the Rabi splitting $\hbar\Omega_R$.

Received: June 22, 2016
Revised: November 9, 2016
Published: November 11, 2016

DOI: 10.1021/acs.nanolett.6b02567
Nano Lett. XXXX, XXX, XXX−XXX

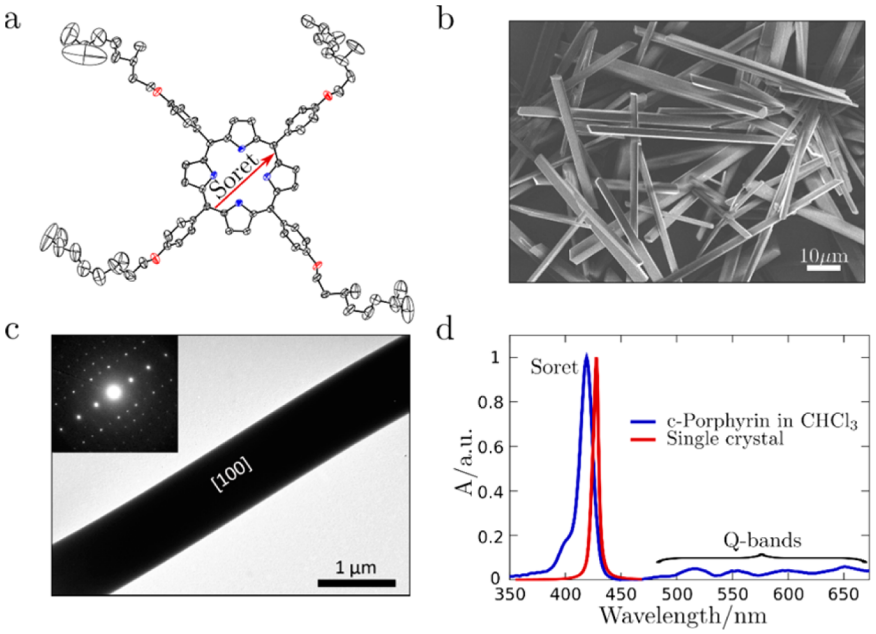

Figure 2. (a) ORTEP drawing of the c-Porphyrin molecule at 50% ellipsoid probability. The red arrow indicates the orientation of the Soret band transition dipole moment. (b) SEM image of an ensemble of single crystal c-Porphyrin nanofibers. (c) TEM image of a typical c-Porphyrin nanofiber and its corresponding SAED image (inset). The fiber axis is identified to be along the crystallographic *a*-axis. (d) Absorbance spectrum of the c-Porphyrin dissolved in $CHCl_3$ (blue curve) and of the single crystal (red curve) as reconstructed from polarized reflectometric measurements.

easily. In this situation, and neglecting the loss terms, the Rabi frequency Ω_R is given by

$$\Omega_R = \vec{d}\cdot\vec{E}\sqrt{N}\sqrt{n_{ph}+1} \quad (1)$$

where $\vec{d}$ is the transition dipole moment of the material, $\vec{E}$ is the electric field per photon in the cavity mode, and n_{ph} is the number of photons in the mode. The last term of this equation implies that even in the absence of any photon, zero point fluctuations of the cavity field can still lead to the eigenstates splitting. Organic dyes strongly coupled to this vacuum field have been extensively studied in recent years as it gives rise to interesting properties such as lasing,[12] Bose−Einstein condensation,[13,14] enhanced conductivity,[15] modified chemical reactivity,[16] and enhanced Raman scattering.[17] Among the many fascinating properties of those systems recently reported,[18,19] the macroscopic coherence that develops in the molecular ensemble upon strong coupling[20,21] and the modification of potential energy surfaces[22] could potentially be extremely valuable in the context of nonlinear optics and nanophotonics.

To date, studies on nonlinear optics involving exciton polaritonic states have focused on their third-order optical nonlinearity and the resulting polariton-polariton interactions.[23] However, the impact of light-matter strong coupling on SHG remains mostly unexplored. To our knowledge, SHG signals from polariton states have only been reported in the context of 2p exciton generation for terahertz lasing devices with GaAs-based microcavities.[24] There it was shown that the relative SHG intensity from |P+> and |P−> depends on the detuning between the quantum dot resonance and the cavity mode, but no quantitative estimation of the polariton SHG efficiency was reported.

Here we study both the efficiency and wavelength dependence of the resonant SHG[25] from strongly coupled single crystalline nanofibers, self-assembled from chiral porphyrin molecules (c-Porphyrin, Figure 2). To ensure the noncentrosymmetric molecular arrangement required for generating second order NLO processes, the model porphyrin molecule was functionalized with four chiral alkyl tails (namely the (*S*)-3,7-dimethyloctyl groups, Figure 2a and Figure S1), and crystallized into nanofibers. As seen in the scanning electron microscope (SEM) image of Figure 2b, those fibers typically have thicknesses of hundreds of nanometers and lengths up to hundreds of micrometers. Selected area electron diffraction (SAED) patterns taken from a typical fiber under a transmission electron microscope (TEM) clearly suggest its single crystalline nature with the fiber axis along the crystallographic *a*-axis (Figure 2c and inset). Moreover, single crystal X-ray diffraction (XRD) of the as-grown bulk crystals suggests that the c-Porphyrin molecules indeed crystallize with a noncentrosymmetric triclinic *P*1 space group (Figure S2), while powder XRD of c-Porphyrin nanofibers suggests that they also share the same crystal phase as shown in the Supporting Information (SI, Figure S3).

When dissolved in chloroform ($CHCl_3$), c-Porphyrin has a sharp Soret absorption band (S_0 to S_2 transition) at 420 nm and Q-bands (S_0 to S_1 transitions) spanning the visible spectrum (Figure 2d, blue curve).[26] The spectroscopic study of the nanofiber crystal phase is experimentally challenging due to the very high extinction coefficient of the Soret band, and the strong optical birefringence ($|n_e - n_o| = 0.2$) and dichroism of the crystal. To measure the single crystal absorption spectrum, we followed a previously reported procedure[27] consisting in refractive index reconstruction from polarized specular reflectance spectroscopy on a single crystal. By probing different polarization angles, we could selectively maximize the Soret or the Q-bands absorption, which is in agreement with their relative orientation (Figure 2a). Throughout the rest of this paper, we always fix the incident polarization to the angle that maximizes the Soret band absorption, which is the targeted transition for strong coupling. The reconstructed absorption

DOI: 10.1021/acs.nanolett.6b02567
Nano Lett. XXXX, XXX, XXX−XXX

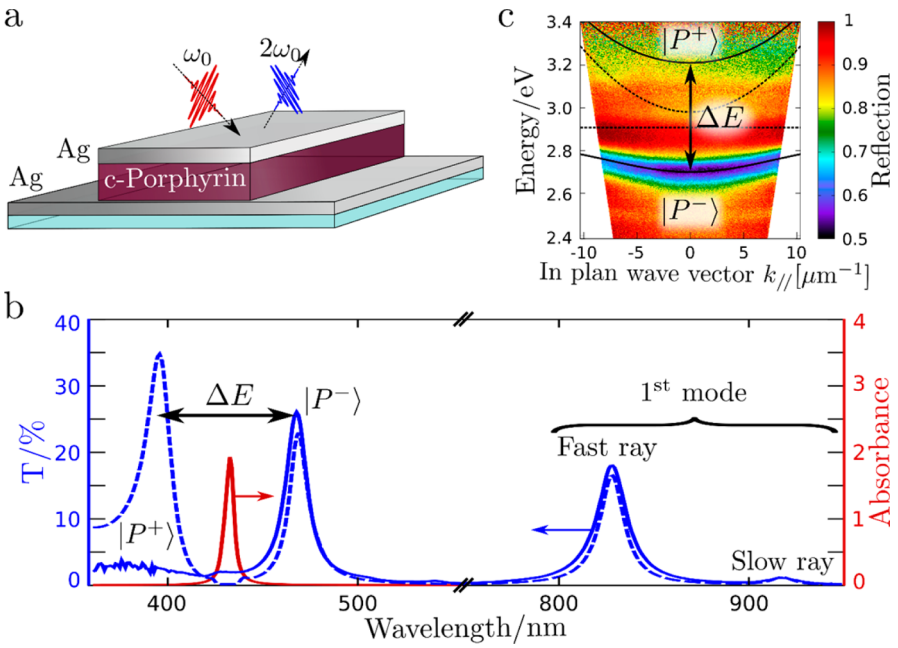

Figure 3. (a) Schematic representation of the nanofiber cavity used for the SHG experiments. (b) Absorbance spectrum of a bare crystal outside the cavity (red curve) and transmission spectrum of a 250 nm thick crystal in the FP cavity (blue curve) with the transfer matrix fit result (dashed blue curve). The two modes in the near IR are the first cavity modes for the two refractive indices of the birefringent crystal. The ratio of their intensities is determined by the chosen polarization. The mode splitting between the two polaritonic states ΔE is ~510 meV. (c) Angle-resolved reflection spectrum of the FP cavity showing the dispersive behavior of the polaritonic states. The solid black curves are coupled oscillators fit to the polaritonic branches, while the dashed ones correspond to the uncoupled exciton and optical resonances.

shows a strong Soret band red-shifted to 430 nm, suggesting a *J*-type aggregation of the c-Porphyrin molecules in line with the crystal XRD observations (Figure S2).

The nanosized molecular crystals were then deposited on a glass substrate coated with a 30 nm thick Ag mirror. Sputtering another 50 nm mirror on top of the crystals led to the formation of Fabry-Pérot (FP) cavities as illustrated in Figure 3a. In this way, a variety of FP cavities were obtained, each defined by the thickness of the embedded c-Porphyrin single crystal (Figure S4) and characterized optically under a microscope. The transmission spectrum was monitored in order to identify a suitable FP cavity with the signature of strong coupling of the Soret band. Figure 3b compares the spectrum of a bare crystal (red curve) with that of the coupled system (blue curve) for a 250 nm thick fiber cavity (Figure S5) displaying a mode splitting ΔE of ~510 meV. Transfer matrix calculations are in very good agreement with the measured spectrum (Figure 3b, blue dashed curve and SI), except for the intensity in the region below 420 nm where the microscope transmits very poorly due to a combination of glass optics and antireflection coatings. Unfortunately, the size of the samples does not allow us to use conventional large beam spectrophotometer to overcome this measurement problem. Moreover, the angle-resolved reflection dispersion spectrum shown in Figure 3c demonstrates the dispersive behavior of the polariton branches. The Rabi splitting, sketched in Figure 1, can be seen in the experimental dispersion Figure 3c as an anticrossing at the in-plane momentum $k_{//} = 0$. From a coupled oscillators fit to the dispersion data (black curves), we extract a resonant Rabi splitting of 500 meV, corresponding to 17% of the Soret transition energy. In this system, the Soret band is coupled to the second optical mode of the cavity. As described below, this has the advantage that the first FP mode in the near-infrared (NIR) can be used as a transparency window to pump the SHG process. By exciting a single c-Porphyrin nanofiber crystal outside the cavity with femto-second pulses at 840 nm (Spectra Physics Mai Tai, 100 fs pulse width, 82 MHz repetition rate), we observe an intense SHG peak at 420 nm (Figure 4a, spectrum indicated by the arrow). The quadratic dependence of this signal on the pump intensity (Figure 4a, inset) and its sharp line width further confirms its second harmonic origin. The SHG spectra recorded for different pumping wavelengths from 740 to 980 nm are shown in Figure 4a. Very importantly, the polarization of the incident laser with respect to the fiber orientation was again set to the angle that maximizes the Soret transition at the second harmonic wavelength. Under those conditions, the wavelength dependent profile of the SHG intensity (Figure 4a) reproduces the Soret absorption band at 430 nm, which is a direct demonstration of the resonance enhanced SHG effect.[25,28]

Performing the wavelength-dependent SHG measurement under the same conditions for a c-Porphyrin nanofiber inside the FP cavity, we obtain a very different intensity profile as shown in Figure 4b. Instead of reaching one maximum at 430 nm, the SHG intensity from the nanofiber in the cavity has two maxima at 390 and 460 nm (pump at 780 and 920 nm) corresponding to resonant SHG from the polaritonic states. Interestingly, the SHG signal from |P−> is more than 5 times larger than that from |P+>. For technical reasons, this wavelength dependence was measured at 45° of incidence angle on a cavity resonantly tuned at that angle. The SHG wavelength dependence was normalized by the cavity filtering function acting on the incident pump beam in the NIR (first cavity mode, as shown in Figure 3b) to correct for the trivial wavelength dependent pumping efficiency. Again, the measured signal grows quadratically with the pump intensity as shown in the inset. Moreover, the polarization-dependent SHG signal, shown in Figure 4c, follows a cosine fourth curve as expected

DOI: 10.1021/acs.nanolett.6b02567
Nano Lett. XXXX, XXX, XXX−XXX

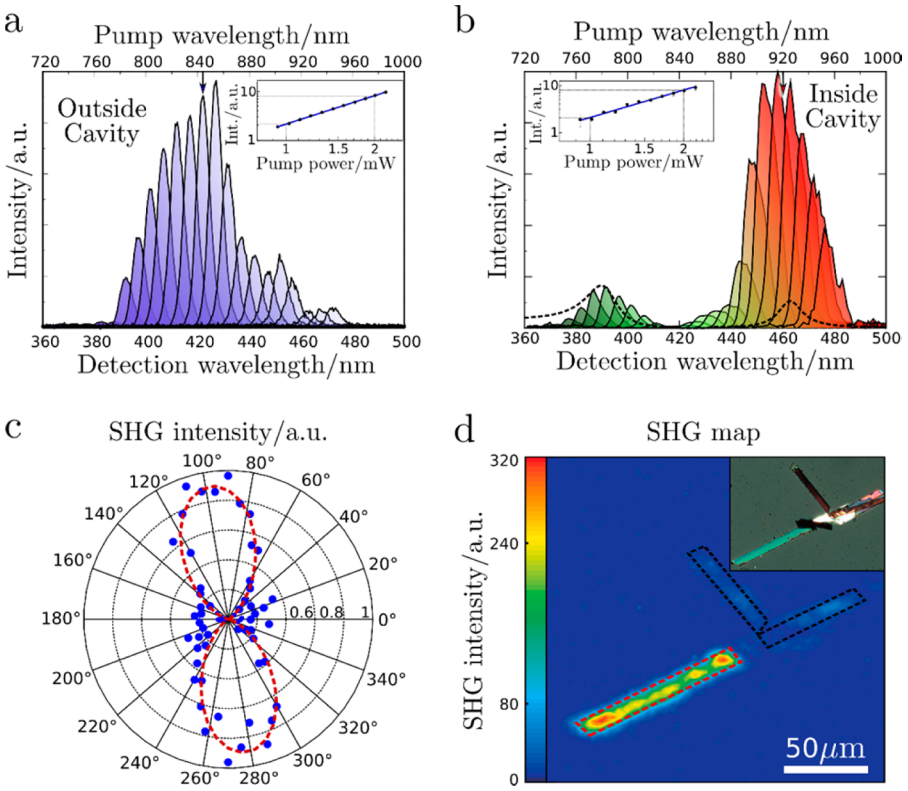

Figure 4. SHG spectra measured at different pump wavelengths for a c-Porphyrin fiber outside (a) and inside (b) the cavity. The cavity data are normalized by the filtering function acting on the pump in the NIR (Figure 3b). The color code is just a visual guide. The dashed curve is the transfer matrix fit to the linear transmission spectrum. The power dependence of the SHG intensity obtained at the wavelength indicated by the arrows in (a,b) are shown in insets (logarithmic plots, black dots) together with fits of slope 2.0 (blue lines). (c) Polar plot of the polarization-dependent SHG signal from the fiber inside the cavity (blue) and its cosine fourth fit (red). (d) SHG intensity scan map (200 × 200 μm^2) of a region around the coupled fiber (red dashed rectangle) and nearby nonresonant fibers (black dashed rectangles). The inset shows the transmission image taken from the same area showing the two thicker fibers (purple in the transmission image) near the resonant fiber (bluish in transmission).

for resonantly enhanced SHG.[7] By raster scanning the sample for a fixed pump wavelength (910 nm), we obtain the SHG intensity map shown in Figure 4d. It clearly outlines the resonant fiber cavity structure (red dashed rectangle), giving a much higher SHG signal than the nearby nonresonant (thicker) Ag-coated fibers imaged in the inset of Figure 4d. This shows that the SHG efficiency is strongly enhanced by the polaritonic states at resonance. It should be noted that the wavelength dependence of Figure 4b cannot be explained by the cavity and its Ag mirrors as the controls in Figure S9 shows.

To better estimate the magnitude of this effect, we now compare the SHG efficiency of c-Porphyrin fibers inside and outside the cavity. A quantitative comparison between those two systems can only be made by accounting accurately for the pump intensity reaching the molecular crystals in both cases. Moreover, the second harmonic field collection efficiency must be precisely computed.[29] For a pump intensity I_ω, the measured second harmonic intensity $I_{2\omega}$ can be written in the electric-dipole approximation as

$$I_{2\omega} \sim (\Gamma_{ex}.\, I_\omega)^2 \cdot J \cdot \Gamma_{det} \tag{2}$$

where Γ_{ex} is the fraction of the pump intensity reaching the material (directly related to the optical mode structure at the pump energy), J contains the second order nonlinear coefficients of the material, and Γ_{det} is the fraction of the second harmonic intensity reaching the detector. Thus, for a fixed pump intensity, the ratio of SHG from inside and outside the cavity reads

$$G = \frac{(I_{2\omega})_{cav}}{(I_{2\omega})_{non\text{-}cav}} = \frac{(\Gamma_{ex}^2.\, J \cdot \Gamma_{det})_{cav}}{(\Gamma_{ex}^2.\, J \cdot \Gamma_{det})_{non\text{-}cav}} = \eta \frac{J_{cav}}{J_{non\text{-}cav}} \tag{3}$$

The estimation of the filtering factors Γ_{ex} and Γ_{det} inside and outside the cavity from transfer matrix calculation (Figures S7 and S8) leads to $\eta = 10^{-2}$. The in situ SHG efficiency J_{cav} exceeds $J_{non\text{-}cav}$ by 2 orders of magnitude (Figure S8), confirming what is qualitatively seen in Figure 4d. It should be stressed that this enhancement stems from a genuine modification of the hybrid states hyperpolarizability since both the pump and harmonic field-enhancement effects have been corrected for in the evaluation of the factor η.

Comparable polaritonic enhancement of the molecular susceptibility has recently been reported for Raman scattering in the regime of vibrational strong coupling (VSC).[17] There, it was argued that the enhancement effect could originate either from the macroscopic coherence that is established in the molecular ensemble by its interaction with a common cavity mode,[20,21] or alternatively from the modification of the nonlinear response at the single molecule level. Even though the energy scales in VSC are reduced by an order of magnitude as compared to electronic strong coupling, the same arguments are indeed also applicable here. In particular, it is striking that for comparable relative coupling strengths, both systems exhibit polaritonic enhancement effects of similar magnitude. Additionally, in both systems the signal at P- dominates that of P+. This suggests a kind of universal behavior in the coherent response of collectively coupled molecular ensembles.

DOI: 10.1021/acs.nanolett.6b02567
Nano Lett. XXXX, XXX, XXX−XXX

This proof of principle that SHG is enhanced for lower exciton polariton opens the door for further studies on the use of strongly coupled systems for NLO of organic materials. The system design needs to be optimized, in particular by using different electromagnetic resonators such as distributed Bragg reflectors, or plasmonic structures where the coupled system is directly accessible, that is, transparent to the pump wavelength. Such structures are however more demanding to design as the orientation of the molecules versus the polarization of the field must be properly aligned. Nevertheless our results indicate that the potential is worth the challenge and could lead to highly efficient NLO organic devices.

■ ASSOCIATED CONTENT

Supporting Information

The Supporting Information is available free of charge on the ACS Publications website at DOI: 10.1021/acs.nanolett.6b02567.

Materials and methods used for synthesis, preparation and characterization of the sample, spectroscopic setups, transfer matrix calculation, SHG efficiency estimations and comparison to a reference cavity (PDF)

■ AUTHOR INFORMATION

Corresponding Authors

*E-mail: jialiang.xu@tju.edu.cn.
*E-mail: ebbesen@unistra.fr.

ORCID

Thomas W. Ebbesen: 0000-0002-3999-1636

Present Address

(C.W.) Center for Advanced Optoelectronic Functional Materials Research and Key Laboratory for UV Light-emitting Materials and Technology of Ministry of Education, Northeast Normal University, Changchun 130024, P.R. China.

Notes

The authors declare no competing financial interest.

■ ACKNOWLEDGMENTS

This work was supported in part by the European Research Council (ERC) "Plasmonics" No. 22577, the ANR Equipex "Union" (ANR-10-EQPX-52-01), the Labex NIE projects (ANR-11-LABX-0058_NIE), USIAS within the Investissement d'Avenir program ANR-10-IDEX-0002-02, The Netherlands Organization for Scientific Research (NWO) with the Veni Grant (680-47-437), the Royal Netherlands Academy of Arts and Sciences (KNAW) with the China-Exchange Program (No. 530-4CDP02), the National Nature Science Foundation of China (NSFC, No. 51503143), the Tianjin Natural Science Foundation (No. 16JCQNJC05000), the Innovation Foundation of Tianjin University (No. 2016XRX-0017), the Tianjin 1000 Youth Talents Plan, the ERC Starting Grant "NANOCAT" No. 259064, and the Chinese Scholarship Council (CSC). A. Toonen and Dr. S. Semin are acknowledged for technical assistance. Dr. J. A. A. W. Elemans is acknowledged for the discussions. G.-J. Janssen from the General Instruments (GI) Department of Radboud University is acknowledged for acquiring the SAED pattern.

■ REFERENCES

(1) Franken, P. A.; Weinreich, G.; Peters, C. W.; Hill, A. E. *Phys. Rev. Lett.* **1961**, *7*, 118.
(2) Sekkat, Z.; Knoll, W. *Photoreactive Organic Thin Films*; Academic Press: San Diego, 2002.
(3) Marder, S. R. *Chem. Commun.* **2006**, *2*, 131.
(4) Sliwa, M.; Nakatani, K.; Asahi, T.; Lacroix, P. G.; Pansu, R. B.; Masuhara, H. *Chem. Phys. Lett.* **2007**, *437*, 212.
(5) Leuthold, L.; Koos, C.; Freude, W. *Nat. Photonics* **2010**, *4*, 535.
(6) Marder, S. R.; Sohn, J. E.; Stucky, G. D. *Materials for Nonlinear Optics: Chemical Perspectives*; American Chemical Society: Washington, DC, 1991; Vol. *455*.
(7) Xu, J.; Semin, S.; Niedzialek, D.; Kouwer, P. H. J.; Fron, E.; Coutino, E.; Savoini, M.; Li, Y.; Hofkens, J.; Uji-I, H.; Beljonne, D.; Rasing, T.; Rowan, A. E. *Adv. Mater.* **2013**, *25*, 2084.
(8) Xu, J.; Semin, S.; Cremers, J.; Wang, L.; Savoini, M.; Fron, E.; Coutino, E.; Chervy, T.; Wang, C.; Li, Y.; Liu, H.; Li, Y. L.; Tinnemans, P.; Kouwer, P. H. J.; Ebbesen, T. W.; Hofkens, J.; Beljonne, D.; Rowan, A. E.; Rasing, T. *Adv. Opt. Mater.* **2015**, *3*, 948.
(9) Xu, J.; Semin, S.; Rasing, T.; Rowan, A. E. *Small* **2015**, *11*, 1113.
(10) Skolnick, M. S.; Fisher, T. A.; Whittaker, D. M. *Semicond. Sci. Technol.* **1998**, *13*, 645.
(11) Houdré, R.; Stanley, R. P.; Oesterle, U.; Ilegems, M.; Weisbuch, C. *Phys. Rev. B: Condens. Matter Mater. Phys.* **1994**, *49*, 16761.
(12) Kéna-Cohen, S.; Forrest, S. R. *Nat. Photonics* **2010**, *4*, 371.
(13) Plumhof, J. D.; Stöferle, T.; Mai, L.; Scherf, U.; Mahrt, R. F. *Nat. Mater.* **2013**, *13*, 247.
(14) Daskalakis, K. S.; Maier, S. A.; Murray, R.; Kéna-Cohen, S. *Nat. Mater.* **2014**, *13*, 271.
(15) Orgiu, E.; George, J.; Hutchison, J. A.; Devaux, E.; Dayen, J. F.; Doudin, B.; Stellacci, F.; Genet, C.; Schachenmayer, J.; Genes, C.; Pupillo, G.; Samorì, P.; Ebbesen, T. W. *Nat. Mater.* **2015**, *14*, 1123.
(16) Hutchison, J. A.; Schwartz, T.; Genet, C.; Devaux, E.; Ebbesen, T. W. *Angew. Chem., Int. Ed.* **2012**, *51*, 1592.
(17) Shalabney, A.; George, J.; Hiura, H.; Hutchison, J. A.; Genet, C.; Hellwig, P.; Ebbesen, T. W. *Angew. Chem., Int. Ed.* **2015**, *54*, 7971.
(18) Ebbesen, T. W. *Acc. Chem. Res.* **2016**, DOI: 10.1021/acs.accounts.6b00295.
(19) Törmä, P.; Barnes, W. L. *Rep. Prog. Phys.* **2015**, *78*, 013901.
(20) Aberra Guebrou, S.; Symonds, C.; Homeyer, E.; Plenet, J. C.; Gartstein, Y. N.; Agranovich, V. M.; Bellessa, J. *Phys. Rev. Lett.* **2012**, *108*, 066401.
(21) Shi, L.; Hakala, T. K.; Rekola, H. T.; Martikainen, J. P.; Moerland, R. J.; Törmä, P. *Phys. Rev. Lett.* **2014**, *112*, 153002.
(22) Galego, J.; Garcia-Vidal, F. J.; Feist, J. *Phys. Rev. X* **2015**, *5*, 041022.
(23) Carusotto, I.; Ciuti, C. *Rev. Mod. Phys.* **2013**, *85*, 299.
(24) Schmutzler, J.; Aßmann, M.; Czerniuk, T.; Kamp, M.; Schneider, C.; Höfling, S.; Bayer, M. *Phys. Rev. B: Condens. Matter Mater. Phys.* **2014**, *90*, 075103.
(25) Heinz, T. F.; Chen, C. K.; Ricard, D.; Shen, Y. R. *Phys. Rev. Lett.* **1982**, *48*, 478.
(26) Gouterman, M. *J. Mol. Spectrosc.* **1961**, *6*, 138.
(27) Anex, B. G. *Mol. Cryst. Liq. Cryst.* **1966**, *1*, 1.
(28) Duan, Y.; Ju, C.; Yang, G.; Fron, E.; Coutino-Gonzalez, E.; Semin, S.; Fan, C.; Balok, R. S.; Cremers, J.; Tinnemans, P.; Feng, Y.; Li, Y.; Hofkens, J.; Rowan, A. E.; Rasing, Th.; Xu, J. *Adv. Funct. Mater.* **2016**, DOI: 10.1002/adfm.201602765.
(29) Ashkin, A.; Boyd, G. D.; Dziedzic, J. *IEEE J. Quantum Electron.* **1966**, *2*, 109.

DOI: 10.1021/acs.nanolett.6b02567
Nano Lett. XXXX, XXX, XXX−XXX